

UC Irvine

Faculty Publications

Title

Tropospheric aerosol impacts on trace gas budgets through photolysis

Permalink

<https://escholarship.org/uc/item/6s22v9bh>

Journal

Journal of Geophysical Research, 108(D8)

ISSN

0148-0227

Authors

Bian, Huisheng
Prather, M J
Takemura, T

Publication Date

2003

DOI

10.1029/2002JD002743

Copyright Information

This work is made available under the terms of a Creative Commons Attribution License, available at <https://creativecommons.org/licenses/by/4.0/>

Peer reviewed

Tropospheric aerosol impacts on trace gas budgets through photolysis

Huisheng Bian and Michael J. Prather

Department of Earth System Science, University of California, Irvine, California, USA

Toshihiko Takemura

Research Institute for Applied Mechanics, Kyushu University, Fukuoka, Japan

Received 10 July 2002; revised 24 October 2002; accepted 10 January 2003; published 22 April 2003.

[1] Aerosols affect the global budgets of O₃, OH, and CH₄ in part through their alteration of photolysis rates and in part through their direct chemical interactions with gases (i.e., “heterogeneous chemistry”). The first effect is evaluated here with a global tropospheric chemistry transport model using recently developed global climatologies of tropospheric aerosols: a satellite-derived aerosol climatology over the oceans by advanced very high resolution radiometer and a model-generated climatology for land plus oceans by the Center for Climate System Research. Globally averaged, the impact of aerosols on photolysis alone is to increase tropospheric O₃ by 0.63 Dobson units and increase tropospheric CH₄ by 130 ppb (via tropospheric OH decreases of 8%). These greenhouse gas increases lead to an aerosol indirect effect (counting both natural and anthropogenic aerosols) of +0.08 W/m². Although the CH₄ increases are, of course, global, the changes in tropospheric OH and O₃ are mainly regional, with the largest impacts in northwest Africa for January and in India and southern Africa for July. The influence of aerosols is greater in July than in January and greater in the Northern Hemisphere than in the Southern Hemisphere, as expected given the pollution sources in the Northern Hemisphere. The predominant impact is due to the aerosols over land; aerosols over the ocean contribute less than a third to globally integrated changes. *INDEX TERMS:* 0305

Atmospheric Composition and Structure: Aerosols and particles (0345, 4801); 0365 Atmospheric Composition and Structure: Troposphere—composition and chemistry; 0368 Atmospheric Composition and Structure: Troposphere—constituent transport and chemistry; 1610 Global Change: Atmosphere (0315, 0325);

KEYWORDS: chemical transport model, tropospheric chemistry, aerosol, photolysis, indirect forcing

Citation: Bian, H., M. J. Prather, and T. Takemura, Tropospheric aerosol impacts on trace gas budgets through photolysis, *J. Geophys. Res.*, 108(D8), 4242, doi:10.1029/2002JD002743, 2003.

1. Introduction

[2] Studies of aerosol influence on tropospheric photolysis and chemical budgets have been conducted in field campaigns and model simulations for individual stations and over regional scales [Dickerson *et al.*, 1997; He and Carmichael, 1999; Balis *et al.*, 2002]. These impacts, however, need to be integrated on a global scale and over decades (i.e., the relaxation time of the CH₄-like mode in global tropospheric chemistry) to assess their importance in trace gas budgets and the greenhouse gas forcing of climate. This gap in the globally integrated impacts of aerosols on photochemistry is due in part to the fact that a global climatology of aerosol properties is not quite ready [Dubovik *et al.*, 2002; Clarke and Kapustin, 2002] and in part to the difficulty in developing an efficient global tropospheric chemistry model that readily includes the effects of clouds and aerosols on photolysis rates. Aerosol properties and

distributions have recently been the focus of intensive investigations through model simulations [Penner *et al.*, 2002; Chin *et al.*, 2002; Takemura *et al.*, 2002], satellite retrievals [Stowe *et al.*, 1997; Mishchenko *et al.*, 1999a; Higurashi *et al.*, 2000; Torres *et al.*, 2002], and field campaigns [Ansmann *et al.*, 2000; Bates *et al.*, 2001; B. Holben, AERONET web page, <http://AERONET.gsfc.nasa.gov>, 2002]. These new aerosol data sets and a newly developed online photolysis model in the University of California Irvine (UCI) global chemistry transport model (CTM) [Wild *et al.*, 2000; Bian and Prather, 2002] make it possible to evaluate the impact of aerosol scattering and absorption on the greenhouse gases CH₄ and O₃.

[3] Ideally, in this evaluation we would use a global, observationally based and hence satellite-derived aerosol climatology, for example, the aerosol products retrieved from the advanced very high resolution radiometer (AVHRR) channel 1 and 2 radiance data [Mishchenko *et al.*, 1999a] (see also the Global Aerosol Climatology Project (GACP) web site at <http://gacp.giss.nasa.gov/>). While these two-channel data provide aerosol optical thickness (AOT)

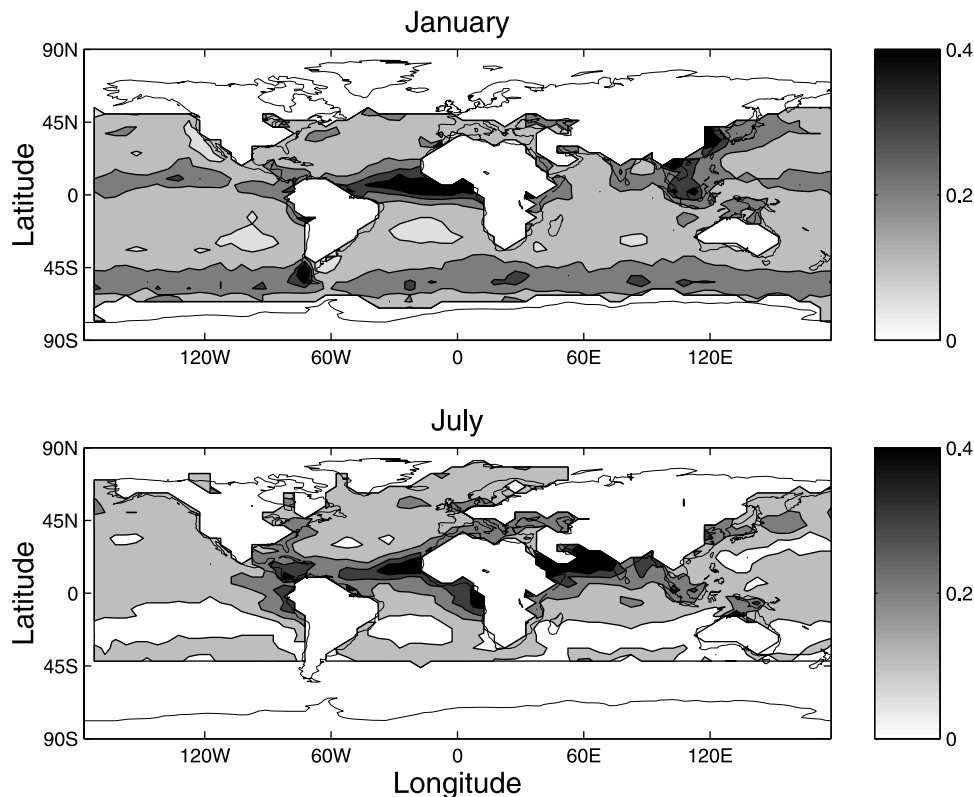


Figure 1. Aerosol optical thickness at 550 nm over oceans averaged over January and over July from the advanced very high resolution radiometer (AVHRR) climatology [Mishchenko *et al.*, 1999a].

and one size parameter, they lack key information on the vertical distribution, the absorptive properties, and the scattering phase function in the ultraviolet-visible region, all of which control the aerosol influence on photochemistry. Further, this product is currently available only over the oceans since retrievals over land are less certain because of variations in surface reflectivity [Knapp and Stowe, 2002]. It is expected that, in time, the Earth Observing System Terra instruments will be able to develop aerosol climatologies that provide much of these key data [Diner *et al.*, 2001; Hook *et al.*, 2001]. As a surrogate for this observational aerosol climatology, we take the aerosol simulations from the Center for Climate System Research (CCSR) [Takemura *et al.*, 2000]. The detailed CCSR climatology provides January and July monthly averages that separate sulfate, sea-salt, dust, and carbonaceous (organic plus black) aerosols. Given the atmospheric abundances, size distributions, and refractive indices for the different aerosol types in three dimensions, it is easy to calculate the optical depth and scattering/absorption properties in each CTM layer. We compare the CCSR and AVHRR climatologies directly with an ocean-only aerosol chemical calculation in which the AVHRR climatology adopts the aerosol optical properties but not the AOT of the CCSR three-dimensional (3-D) product.

[4] The two aerosol climatologies are described and compared in section 2. The UCI CTM and the methodology of the different chemical simulations are presented in section 3. We analyze the impact of aerosols on the tropospheric burdens of O_3 , OH, CH_4 , and some odd nitrogen

species in section 4. In the concluding section 5 we estimate that the photolytic effect of aerosols (natural plus anthropogenic) on the greenhouse gases CH_4 and O_3 is +5–10% of the change since the preindustrial era and amounts to $+0.08 \text{ W/m}^2$.

2. Aerosol Climatologies

[5] An aerosol climatology over oceans has been derived from the AVHRR satellite radiances at channel 1 ($\lambda = 650 \text{ nm}$) and channel 2 ($\lambda = 850 \text{ nm}$) [Mishchenko *et al.*, 1999a] using monthly averages from the period February 1985 through October 1988. This two-channel algorithm works only over oceans (uniformly dark surfaces) and provides more accurate and less biased retrievals of the AOT than the one-channel algorithm. It also provides some information on aerosol size through the Angstrom parameter, defined as the exponential dependence of AOT on wavelength between the two channels. Figure 1 shows the total AOT at 550 nm for the AVHRR ocean aerosol in January and July. No consolidated satellite climatology for land-plus-ocean aerosol was available from the GACP for this study. The CCSR model simulations [Takemura *et al.*, 2000] of AOT for each aerosol type (dust, carbonaceous, sulfate, and sea-salt) are available only for January and July. Figure 2 shows the CCSR 550 nm AOT in both January and July for the sum of all aerosol types.

[6] A summary comparison of the two aerosol climatologies is given in Table 1, where the ocean-only AOT for July is averaged over regions and CCSR AOT is further

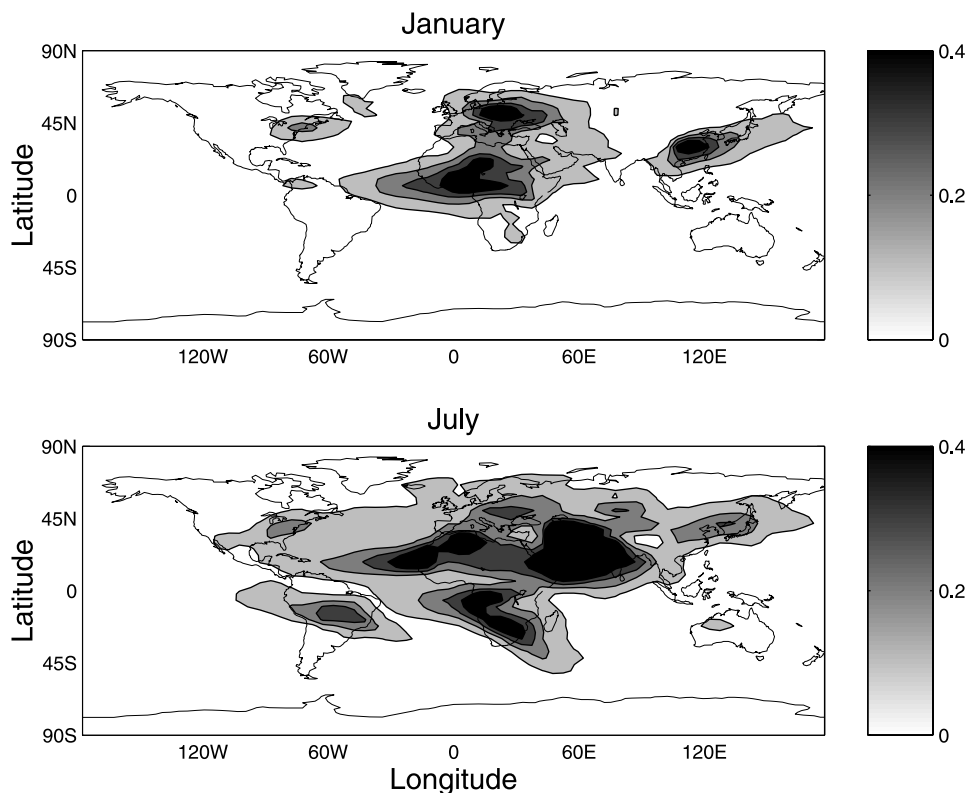


Figure 2. Total aerosol optical thickness (sum of sea-salt, sulfate, dust, and carbonaceous aerosols) at 550 nm averaged over January and over July for the Center for Climate System Research (CCSR) model [Takemura *et al.*, 2000].

separated by aerosol type. Differences appear largest over the remote ocean, where the CCSR predicts a factor of ~ 2 less than AVHRR retrievals. Kinne *et al.* [2003] present a global comparison among seven models, three satellite data sets, and the Aerosol Robotic Network data, focusing on monthly averages of aerosol properties. They report that model simulations are usually smaller than satellite-derived values, especially when comparing to Total Ozone Mapping Spectrometer data and AVHRR data in remote regions. Furthermore, they point out that CCSR low predicted AOT in remote regions is likely caused by either weak transport or strong removal of dust, carbonaceous, and sulfate aerosols combined with weak mass extinction efficiency of sea salt. Over oceanic regions affected by land aerosol sources the CCSR AOT is equivalent or slightly higher, and over the northern Indian Ocean it is more than twice the AVHRR AOT. In these regions, near combustion and biomass burning sources, the CCSR aerosol extinction for carbonaceous aerosols (including organic and black) is much greater than in remote regions. Although the CCSR AOT in remote oceans is much smaller than the AVHRR, the areas affected by land sources have a larger weighting in estimating the global mean ocean AOT. Thus the global oceanic mean AOT from CCSR is only slightly less than the AVHRR retrieval in July.

[7] The CCSR climatology specifies the 3-D aerosol extinction at 550 nm by type, but we must still adopt an aerosol model (size distribution and index of refraction) to derive the optical properties used to calculate photolysis

rates [Wild *et al.*, 2000]. Specifically, the single-scattering albedo and the first seven coefficients in the Legendre expansion of the scattering phase function for ultraviolet and visible wavelengths (300–600 nm) are needed. For each CCSR type (sulfate, carbonaceous, dust, and sea-salt) we adopt an index of refraction (n) (wavelength independent) and lognormal size distribution (r_g and σ) based on atmospheric measurements [Twitty and Weinman, 1971; Volz,

Table 1. Comparison of Ocean AOT at 550 nm for July Between Satellite AVHRR Retrieval and the CCSR Model^a

Ocean Regions	AVHRR ^b Total AOT	CCSR ^c AOT				
		Total	Carbonaceous	Sulfate	Sea-Salt	Dust
Global oceans	0.16	0.13	0.037	0.036	0.016	0.044
NH oceans	0.19	0.17	0.026	0.057	0.012	0.077
SH oceans	0.12	0.085	0.05	0.010	0.021	0.004
East Pacific (NH)	0.14	0.048	0.006	0.023	0.010	0.008
West Pacific (NH)	0.14	0.086	0.013	0.049	0.009	0.014
East Pacific (SH)	0.11	0.045	0.016	0.006	0.021	0.002
Indian (SH)	0.09	0.064	0.028	0.007	0.024	0.006
Atlantic (equator)	0.29	0.32	0.14	0.042	0.015	0.13
Pacific/East Asia	0.16	0.22	0.046	0.12	0.008	0.046
Indian (NH)	0.43	1.08	0.059	0.10	0.022	0.90

^aAbbreviations are as follows: AOT, aerosol optical thickness; AVHRR, advanced very high resolution radiometer; CCSR, Center for Climate System Research; NH, Northern Hemisphere; and SH, Southern Hemisphere.

^bAVHRR retrieval is by Mishchenko *et al.* [1999a].

^cThe CCSR model was generated by Takemura *et al.* [2000].

Table 2. Aerosol Radiative Properties Adopted for CCSR Types as a Function of Wavelength (λ)^a

λ , nm	Q	r_{eff}	ω^0	ω^1	ω^2	ω^3	ω^4	ω^5	ω^6	ω^7
<i>Sulfate</i> ($n = 1.45 - 0.0037i$; Lognormal $r_g = 90$ nm, $\sigma = 0.6$)										
300	2.7040	0.224	0.9702	2.212	2.829	2.764	2.568	2.213	1.861	1.554
400	2.3984	0.224	0.9749	2.198	2.683	2.525	2.181	1.774	1.381	1.079
600	1.6009	0.224	0.9770	2.101	2.410	2.066	1.639	1.203	0.863	0.612
999	0.7455	0.224	0.9738	1.898	1.958	1.460	1.015	0.651	0.416	0.260
<i>Carbonaceous</i> ^b ($n = 1.80 - 0.30i$; Lognormal $r_g = 140$ nm, $\sigma = 0.37$)										
300	2.8113	0.198	0.4943	2.363	3.152	3.389	3.249	2.892	2.400	1.919
400	2.9349	0.198	0.5104	2.213	2.635	2.524	2.088	1.601	1.124	0.755
600	2.7167	0.198	0.5224	1.933	1.861	1.394	0.884	0.497	0.268	0.133
999	1.7662	0.198	0.4726	1.483	1.100	0.537	0.226	0.078	0.027	0.009
<i>Dust</i> ($n = 1.5 - 0.025i$; Lognormal $r_g = 250$ nm, $\sigma = 0.79$)										
300	2.3972	1.182	0.6339	2.552	3.847	4.810	5.783	6.561	7.342	7.987
400	2.4507	1.182	0.6709	2.469	3.606	4.346	5.092	5.631	6.172	6.570
600	2.5593	1.182	0.7244	2.349	3.293	3.735	4.166	4.396	4.613	4.741
999	2.6365	1.182	0.7902	2.260	2.978	3.118	3.202	3.119	3.030	2.912
<i>Sea Salt</i> ($n = 1.5 - 0.003i$; Lognormal $r_g = 300$ nm, $\sigma = 0.4$)										
300	2.6056	0.452	0.9437	2.029	2.951	2.962	3.502	3.420	3.767	3.754
400	2.8618	0.452	0.9608	2.044	2.795	2.739	2.976	2.795	2.799	2.623
600	3.1537	0.452	0.9771	2.098	2.725	2.587	2.422	2.053	1.703	1.382
999	2.6244	0.452	0.9844	2.111	2.449	2.110	1.646	1.160	0.781	0.498

^aSee text. Extinction efficiency Q and area-weighted mean radius r_{eff} are diagnostic and are not used in photolysis calculations.

^bCarbonaceous includes both organic and black carbon.

1972; Ward et al., 1973; Grams et al., 1974; Hsu et al., 1999; Ji et al., 2000; Diaz et al., 2001]. This model is summarized in Table 2 along with the optical properties as a function of wavelength calculated from Mie theory: the single-scattering albedo (ω_0) and Legendre expansion of the scattering phase function (ω^i , $i = 0, \dots, 7$). Also given are diagnostic quantities, the extinction efficiency (Q) (mean extinction cross section over cross-sectional area), and the effective radius (r_{eff}) (area-weighted mean radius). The detailed properties at 999 nm are not important in photolysis but are included because Fast-J can then scale AOT reported at 1μ (e.g., stratospheric sulfate aerosols). Note that we use our aerosol model (i.e., $Q(\lambda)$) rather than the Angstrom coefficient to calculate the AOT climatologies from 550 nm to the critical wavelength range for tropospheric photochemistry (300–400 nm). In combining extinction from different aerosol types (and sometimes clouds) in a CTM layer we assume an external mixture.

[8] The AVHRR ocean climatology is only two-dimensional (2-D) and lacks both vertical distribution and speciation. We must make several assumptions to use it in the CTM. For speciation we assume an external mixture and use the CCSR climatology to calculate an average index of refraction over each ocean grid cell in the CTM, weighting the indices of refraction in Table 2 by the CCSR 550-nm AOT for each type. We calculate the optical properties for each grid cell by combining this mean index of refraction with a modified bimodal lognormal distribution using the AVHRR-specific parameterization [Mishchenko et al., 1999b; Higurashi et al., 2000] that includes variation in the fraction of large particles as a function of AOT. The vertical distribution of aerosol extinction for the AVHRR climatology was set proportional to the local water vapor density in the CTM.

[9] The aerosol refractive index determines the single-scattering albedo and is a key parameter controlling photolysis rates. It must be regarded as a major uncertainty in this investigation. We adopt a smaller imaginary refractive index (0.003) than the previous value (0.005) for sea salt recommended by a recent study (I. Geogdzhayev, personal communication, 2000). A sensitivity study using AVHRR climatology examines a range in aerosol absorption. Both carbonaceous aerosols and desert dust absorb strongly in the wavelength range of 300–400 nm, while sea-salt and sulfate aerosols absorb very little. Since we chose a wavelength-independent index of refraction, we keyed this value for dust aerosol to give a single-scattering albedo in the photochemical region (300–400 nm) of ~ 0.66 . According to recent studies on mineral dust over the tropical North Atlantic Ocean the single-scattering albedo of dust at wavelengths < 400 nm can be < 0.6 , but it increases rapidly for wavelengths > 550 nm [Savoie et al., 2000; Ji et al., 2000]. Some other studies [Diaz et al., 2001; Kaufman et al., 2001; Dubovik et al., 2002] about single-scattering albedo over or toward the photochemical spectrum also support our standard model in Table 2. On the other hand, He and Carmichael [1999] give a single-scattering albedo for Saharan dust as 0.77 (independent of wavelength) in their calculations of photolysis rates. Thus we consider an alternative model of moderate dust absorption (mod D) with a lower imaginary refractive index that raises the single-scattering albedo at 300 nm from 0.62 (using the AVHRR size distribution and the CCSR index of refraction) to 0.72. Hsu et al. [1999] and Twitty and Weinman [1971] suggest three different refractive indices for carbonaceous aerosols to represent weak (single-scattering albedo of 0.9 at 300–400 nm), moderate (0.8), and strong (0.5, the standard model) absorption depending on the fraction of black versus organic carbon. We combine the moderate dust absorption alternative with moderate and weak carbonaceous absorption to define two alternative models, mod C and weak C, with successively less absorption. Finally, we consider that all AOT over the ocean is sea salt with minimal absorption (0.95 at 300–400 nm).

3. Tropospheric Chemistry Simulations

[10] The three-dimensional global chemical transport model at UCI can be driven by different meteorological fields. The meteorological fields used in this study are from the Goddard Institute for Space Studies (GISS) general circulation model version II that is run with a resolution of 4° latitude, 5° longitude, and nine vertical layers. These meteorological fields include 3-D (winds, temperature, water vapor, clouds, and convection) and 2-D (boundary layer properties) data at 3-hour averages. The CTM resolution matches that of these GISS meteorological fields and includes an O_3 - NO_x -NMHC chemical scheme with 36 species, 88 chemical kinetic reactions, and 22 photolytic reactions [Wild and Prather, 2000; Wild and Akimoto, 2001; Bian, 2001]. Trace gas emissions are based on the Global Emissions Inventory Activity database [Benkovitz et al., 1996], with updated totals from the Intergovernmental Panel on Climate Change (IPCC) third assessment [Prather and Ehhalt, 2001]. A first-order rainout parameterization for soluble gases is used for large-scale precipitation [Giorgi

and *Chameides*, 1986], and scavenging in convective precipitation is built in to the convective mass transport operator [Bian, 2001]. Dry deposition of gases is calculated with a resistance-in-series scheme [Jacob *et al.*, 1992]. The numerical solution for advection and convection conserves the second-order moments of tracer distribution (i.e., quadratics plus cross terms). The UCI CTM had been applied previously to the simulations of both tropospheric and stratospheric chemistry and transport [Prather *et al.*, 1987; Hall and Prather, 1993; Avallone and Prather, 1997; Jacob *et al.*, 1997; Hannegan *et al.*, 1998; Olsen *et al.*, 2000; McLinden *et al.*, 2000]. The tropospheric model has been evaluated recently in several publications: tropospheric O₃ and CO, NO_x/NO_y species at Mauna Loa, and global peroxyacetylnitrate (PAN) profiles of Wild and Prather [2000] and Wild and Akimoto [2001], further O₃ and CO evaluations of IPCC 2001 [Prather and Ehhalt, 2001], and updated radon and lead simulations of Bian [2001].

[11] Aerosols are included here in the calculation of photolysis rates using the multiple-scattering Fast-J scheme [Wild *et al.*, 2000; Bian and Prather, 2002], which explicitly accounts for aerosol and cloud optical properties. In each CTM layer the monthly mean aerosol extinction is combined with the 3-hour cloud optical depths from the meteorological fields. Fast-J is computationally efficient, and the radiation field as a function of wavelength is calculated hourly throughout the entire column. Tropospheric photolysis is calculated from seven variable-width wavelength bins between 289 and 850 nm. Atmospheric absorption and scattering include O₂ and O₃ absorption, Rayleigh scattering, water cloud and ice cloud absorption and scattering, and aerosol absorption plus scattering.

[12] Calculating the impact of a perturbation to tropospheric chemistry alone would require several decades of continuous simulation to allow for CH₄ to respond. If stratospheric chemistry were included, this time would be centuries. For these exploratory studies we restrict ourselves to tropospheric chemistry and use several approximations to calculate the aerosol impact. The CTM control case is run without aerosols. For some sensitivity studies we use very short, 2-month simulations: We begin 1 June with the same initialization as the control run, impose different aerosol models, integrate through 31 July, and then diagnose the changes averaged over July. These simulations give us a quick look at the relative impact of differing assumptions, but the absolute numbers cannot be used quantitatively. While the 1-month spin-up allows for O₃, OH, H₂O₂, and most odd nitrogen species to come close to steady state, the perturbation to other key gases like CO and C₂H₆ is still far from steady state, and their approach to steady state will continue to change O₃ and OH. For our budget studies we complete a 19-month, full seasonal CTM simulation beginning 1 July year 1 (from a much longer run) and ending 31 January year 3. Owing to the lack of a continuous climatology from CCSR we ran two perturbation budget studies: one with a perpetual January CCSR climatology and the other with a perpetual July CCSR climatology. Examples of changes in trace gases and budgets are derived from January year 3 (using January aerosols) and July year 2 (using July aerosols). The minimum 12-month spin-up time of these runs allows for most chemically important trace gases, except CH₄, to settle close to steady state. These budgets

are then used to project the steady state CH₄ perturbation, including its feedback upon its own lifetime as per recent assessments [Prather and Ehhalt, 2001].

4. Results

[13] Changes in tropospheric O₃ caused by the interaction of aerosols with the ultraviolet and visible radiation field are shown in Figure 3 for January and July. Results are plotted from the budget runs for the first six CTM model levels as CCSR aerosols minus control run for O₃ and divided by control run further for OH. Note that CH₄ is evolving slowly in these simulations, and hence the change in O₃ does not include the effects of the CH₄ perturbation (diagnosed below) that would add ~0.4 ppb globally to these figures.

[14] For tropospheric O₃ the inclusion of the aerosols leads to an increase of about +1 ppb over most of the globe, but regionally this change can vary from less than -15 to more than +2 ppb in January and from -10 to +3 ppb in July. In the low-aerosol regions this increase is slightly large in the summer hemisphere. In regions with lower aerosol loading O₃ perturbations are between ±2 ppb in both January and July; in regions with high aerosol loading, particularly absorbing aerosol, O₃ abundances are suppressed by >2 ppb. This fits with previous studies that report O₃ reductions in the lower atmosphere due to the presence of absorbing aerosols [Jacobson, 1998; He and Carmichael, 1999]. These O₃ reductions are the largest and appear to be created in the lower troposphere. They are manifest in the upper troposphere and downwind by convective and advective transport. In our model the reduced O₃ occurs primarily over high-NO_x, continental, ozone-producing regions and is driven by the general reduction in photolysis rates, resulting in less photochemical formation of O₃. Over the low-NO_x oceanic regions, O₃ is being destroyed by photochemistry [Olson *et al.*, 1997], and hence the presence of absorbing aerosols (e.g., over the tropical Atlantic) reduces this loss, resulting in O₃ increases of >2 ppb or more. On average, aerosols tend to reduce the photochemical loss of O₃ in the boundary layer and lead to the global background increase of <1 ppb. The largest ozone changes are coincident with dust (Sahara and Arabia) and biomass burning aerosols (South America and Africa). Note that O₃ loss over Europe in January is small even though aerosol loading is high (see Figure 2). In Europe the AOT is dominated by sulfate aerosol with very low absorptivity, and, further, the wintertime photochemical production of O₃ in midlatitudes is low. In July, with photochemical production in the continental boundary layer becoming important, aerosol scattering is seen to decrease O₃ over North America and Europe, although this effect does not impact much beyond the boundary layer.

[15] Changes to tropospheric OH caused by aerosols are shown in Figure 4 for January and July. The global patterns are similar to those for O₃ but, interestingly, there are no regions of significant increase. Over most of the globe, OH decreases are <10%; however, tropospheric OH decreases by >30% over west Africa in January and by >50% over the north Indian Ocean in July. In general, OH decreases are driven by reductions in ultraviolet photolysis of O₃ to form O(¹D), the primary source of OH. Other photochemical

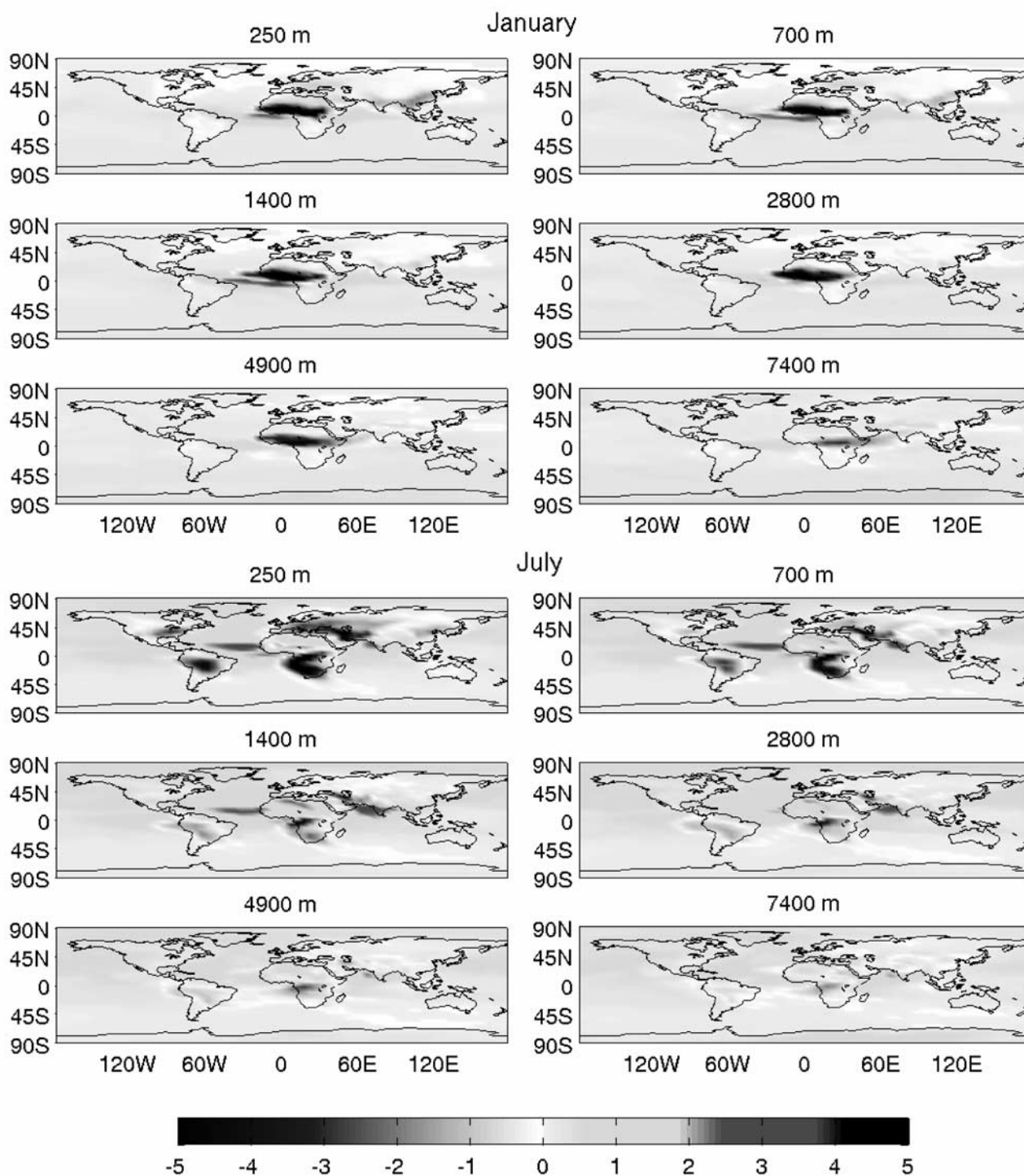


Figure 3. Perturbations to O₃ (ppb) by global aerosol at six atmospheric layers in January and July. See color version of this figure at back of this issue.

changes augment this, for example, reductions in NO alter the balance between OH and HO₂, favoring the latter. In addition, decreases in OH have a positive feedback in that the resulting increases in CO lead to further OH decreases. As noted for O₃ below, the CH₄ perturbation in these runs is far (>90%) from steady state, and if we project the CH₄ perturbation, there is an additional OH decrease of 2%. The OH decreases are larger and show more horizontal inhomogeneity in the lower

troposphere than in the upper atmosphere, reflecting the rapid photochemical response of OH to local conditions. When only scattering is considered, as in *Berntsen and Isaksen's* [1997] study of the impact of clouds on upper tropospheric chemistry, the calculated OH abundances are larger above clouds than for clear-sky conditions. Thus it is clear that aerosol absorption rather than scattering is driving these global OH decreases.

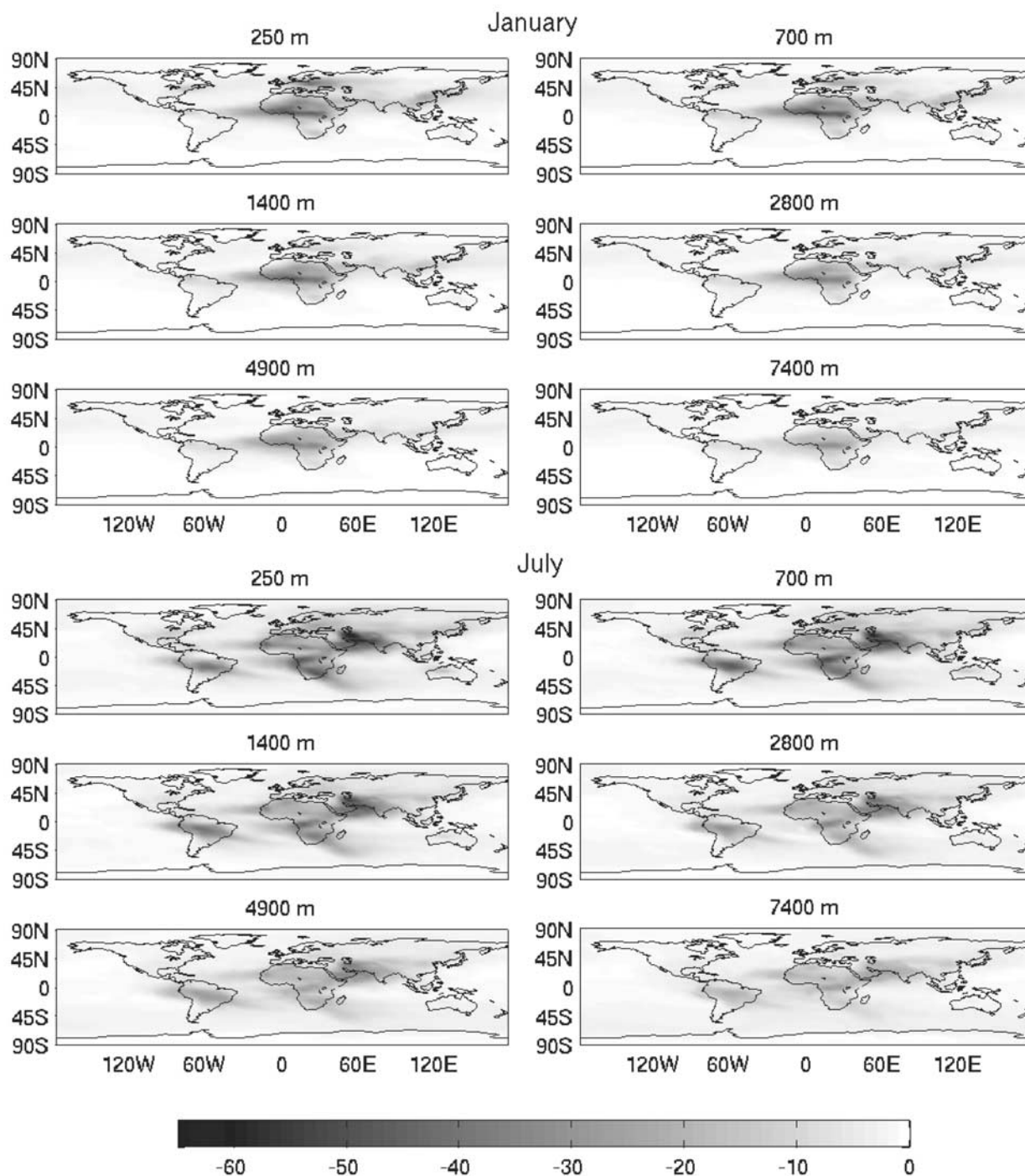


Figure 4. Perturbations to OH (%) by global aerosol at six atmospheric layers in January and July.

[16] Sensitivity tests with only 1-month spin-up are used to assess the relative global importance of different aerosol models. The average July perturbations to the global burdens of tropospheric O_3 , NO, NO_2 , PAN, and OH following a 1 June initialization are summarized in Table 3. For the CCSR climatology the aerosols over the oceans (70% of the surface) are responsible for only 20–40% of the total perturbation. The ocean-only climatologies of CCSR and AVHRR for July yield similar perturbations, although those

of AVHRR are systematically larger as expected from their slightly larger AOTs. The importance of aerosol absorptivity is demonstrated with the ocean-only AVHRR sequence using different models for the refractive index (see discussion in section 2). Reducing the dust absorption by a third (mod D) has little impact. By additionally reducing the carbonaceous absorptivity to a single-scattering albedo of 0.8 (mod C) and 0.9 (weak C), the aerosol impact is reduced by a factor of 3. Using a sea-salt model for all oceanic

aerosols results in a negligible impact. Thus the land aerosols dominate, and it is the absorptivity of the carbonaceous and dust aerosols that drives the changes in tropospheric photochemistry.

5. Projections and Conclusions

[17] The budget lifetime of CH₄ in this CTM is 9.6 years, and the e-folding time of a perturbation is ~14 years [Wild and Prather, 2000]. We use this knowledge of the chemical modes and the CH₄ feedbacks diagnosed from many CTMs to project these aerosol perturbations to a steady state. Table 4 summarizes the increase in CH₄ lifetime, the decrease in tropospheric OH burden, and the increase in tropospheric O₃ burden for January and July budget runs as caused by aerosol impacts on photolysis. The northern summer dominates by more than a factor of 2. We estimate an annual average from these two months (e.g., a 5.6% increase in CH₄ lifetime) and use the IPCC 2001 results from an ensemble of CTMs [Prather and Ehhalt, 2001] to estimate the feedbacks when the CH₄ perturbation reaches steady state. These feedbacks augment the mean tropospheric OH perturbation by a factor of 1.4 and predict that the CH₄ abundance is ~130 ppb higher with aerosols than without. The tropospheric O₃ burden is greatly amplified by this increase in CH₄ from 0.25 to 0.63 Dobson units. In summary, the impact of aerosols on photolysis alone is to increase tropospheric O₃ by ~1 ppb and to increase tropospheric CH₄ by ~130 ppb (via tropospheric OH decreases of ~8%). These greenhouse gas increases produce an increase in radiative forcing of ~0.08 W/m².

[18] In this paper we calculate global aerosol-photolysis coupling using a photolysis model (Fast-J) within the UCI CTM that couples aerosol and cloud layers. The results clearly show impacts at the 5–10% level for global tropospheric chemistry, but regional perturbations can be as large as 50%, for example, in OH abundances. Perturbations are largest in the lower troposphere, over the continents, and generally in the summer hemisphere. This aerosol impact is dominated by the highly absorbing aerosols (carbonaceous and dust). The global results here may be a lower bound because they use the CCSR model climatology that over the ocean generally underestimates the satellite-derived AOT from AVHRR. We intend to work with the next generation

Table 3. Sensitivity Studies of Global Mean Chemical Perturbations Based on Short-Term Simulations for July From CCSR (Land-Plus-Ocean and Ocean-Only) and AVHRR (Ocean-Only)^a

Global Mean	CCSR		AVHRR				
	Global	Ocean	Ocean (Std)	(Mod D)	(Mod C)	(Weak C)	(Sea Salt)
O ₃ , DU	+0.30	+0.13	+0.19	+0.15	+0.09	+0.07	+0.04
NO, %	-2.4	-0.5	-1.6	-1.6	-0.8	-0.6	-0.4
NO ₂ , %	+6.5	+1.4	+2.2	+2.2	+1.0	+0.7	+0.3
PAN, %	+9.4	+2.9	+3.3	+3.3	+1.5	+1.0	+0.4
OH, %	-8.1	-2.4	-4.9	-4.9	-1.5	-0.8	-0.3

^aFor AVHRR the standard model is compared with uncertainties in the refractive index: moderate dust absorption, moderate and weak carbonaceous absorption, and sea salt only (see text). Definitions are as follows: Std, standard absorption model; mod D, moderate dust absorption model; mod C, moderate carbonaceous absorption model; weak C, weak carbonaceous absorption model; and DU, Dobson units.

Table 4. Global Mean Changes in Tropospheric Chemistry Driven by Aerosol Impacts on Photolysis Rates^a

	Global	January	July	Annual	CH ₄ Feedback	Steady State
CH ₄ lifetime, %	+3.6	+7.6	+5.6	+2.2	+7.8	
Mean OH, %	-3.9	-7.9	-5.9	-2.3	-8.2	
Mean O ₃ , DU	+0.14	+0.36	+0.25	+0.38	+0.63	

^aCalculations for the CCSR climatologies for January and July are averaged to estimate the annual change. Additional projected CH₄ feedbacks at steady state are based on values given by Prather and Ehhalt [2001] and predict that without aerosols, CH₄ would be ~130 ppb lower.

of satellite climatology [Mishchenko et al., 2002], which will consolidate ocean and land AOT to reduce this uncertainty.

[19] The monthly mean aerosol climatologies here are used in conjunction with a 3-hour meteorological field of varying cloud layers. Generally, the aerosols have maximal impact on photochemistry in cloud-free conditions. If the cloud fields and aerosols are correlated, then our assumption of constant AOT for variations in cloud cover may induce errors. For AVHRR the climatology is based on cloud-free conditions, and thus there should be minimal systematic bias in these simulations. Uncertainties in aerosol composition, radiative properties, and vertical distribution all affect tropospheric photolysis. For example, we assume that the aerosol vertical distribution of AVHRR climatology is proportional to the local water vapor density in the CTM. This assumption is perhaps fine for sulfate but is wrong for dust, which is generally transported in a dry layer above the boundary layer. The aerosol vertical profiles are the most poorly known data in aerosol research. In addition, refractive indices vary with wavelength. Therefore the wavelength-independent indices adopted in our study, although they represent well the mean values in the key tropospheric chemical spectrum, will induce the error in photolysis calculation. A next step would be to couple a full aerosol model with the tropospheric CTM to resolve issues of variability and to correlate anthropogenic aerosols with trace gas pollutants. We believe that this study demonstrates the necessity for coupled aerosol-chemistry models to use a Fast-J or equivalent model that couples aerosols with clouds and ozone in calculating photolysis.

[20] Aerosols also impact tropospheric photochemistry through gas-aerosol (heterogeneous) reactions, and many different types of heterogeneous reactions have been studied [Dentener and Crutzen, 1993; Dentener et al., 1996; Lary et al., 1996; Wahner et al., 1998; Lary et al., 1999; Knipping et al., 2000; Jacob, 2000; Tie et al., 2001; Underwood et al., 2001]. For example, the impact of aqueous phase reactions of HNO₄ [Dentener et al., 2002] appears to be comparable to the photolytic impacts shown here, although photolytic changes in OH extend throughout most of the troposphere. However, such evaluations are even more uncertain than this one because the detailed chemical composition and mixture of the aerosols, which plays a great role in heterogeneous chemistry, is even more difficult to extract from the observed climatology.

[21] **Acknowledgments.** We thank the NASA Global Aerosol Climatology Project for its support of this research. We are grateful to the entire GACP team and particularly to M. Mishchenko and I. Geogshayev for their help with aerosol climatologies and their program to compute optical properties of aerosols. We also thank O. Wild for his helpful comments.

This thesis work was funded by the NASA and NSF atmospheric chemistry programs.

References

- Ansmann, A., D. Althausen, U. Wandinger, K. Franke, D. Müller, F. Wagner, and J. Heintzenberg, Vertical profiling of the Indian aerosol plume with six-wavelength lidar during INDOEX: A first case study, *Geophys. Res. Lett.*, **27**, 963–966, 2000.
- Avallone, L. M., and M. J. Prather, Tracer-tracer correlations: Three-dimensional model simulations and comparisons to observations, *J. Geophys. Res.*, **102**, 19,233–19,246, 1997.
- Balis, D. S., C. S. Zerefos, K. Kourtidis, A. F. Bais, A. Hofzumahaus, A. Kraus, R. Schmitt, M. Blumthaler, and G. P. Gobbi, Measurements and modeling of photolysis rates during the Photochemical Activity and Ultraviolet Radiation (PAUR) II campaign, *J. Geophys. Res.*, **107**(D18), 8138, doi:10.2029/2000JD000136, 2002.
- Bates, T. S., et al., Regional physical and chemical properties of the marine boundary layer aerosol across the Atlantic during Aerosols99: An overview, *J. Geophys. Res.*, **106**, 20,767–20,782, 2001.
- Benkovitz, C. M., M. T. Scholtz, J. Pacyna, L. Tarrasón, J. Dignon, E. C. Voldner, P. A. Spiro, J. A. Logan, and T. E. Graedel, Global gridded inventories of anthropogenic emissions of sulfur and nitrogen, *J. Geophys. Res.*, **101**, 29,239–29,253, 1996.
- Berntsen, T. K., and I. S. A. Isaksen, A global three-dimensional chemical transport model for the troposphere, 1, Model description and CO and ozone results, *J. Geophys. Res.*, **102**, 21,239–21,280, 1997.
- Bian, H., Improvement and application of UCI chemistry transport model, Ph.D. thesis, 310 pp., Univ. of Calif., Irvine, Calif., 2001.
- Bian, H., and M. J. Prather, Fast-J2: Accurate simulation of stratospheric photolysis in global chemistry models, *J. Atmos. Chem.*, **41**, 281–296, 2002.
- Chin, M., et al., Tropospheric aerosol optical thickness from the GOCART model and comparisons with satellite and Sun photometer measurements, *J. Atmos. Sci.*, **59**, 461–483, 2002.
- Clarke, A. D., and V. N. Kapustin, A Pacific aerosol survey, part I: A decade of data on particle production, transport, evolution, and mixing in the troposphere, *J. Atmos. Sci.*, **59**, 363–382, 2002.
- Dentener, F. J., and P. J. Crutzen, Reaction of N₂O₅ on tropospheric aerosols: Impact on the global distributions of NO_x, O₃, and OH, *J. Geophys. Res.*, **98**, 7149–7163, 1993.
- Dentener, F. J., G. R. Carmichael, Y. Zhang, J. Lelieveld, and P. J. Crutzen, Role of mineral aerosol as a reactive surface in the global troposphere, *J. Geophys. Res.*, **101**, 22,869–22,889, 1996.
- Dentener, F. J., J. Williams, and S. Metzger, Aqueous phase reaction of HNO₄: The impact on tropospheric chemistry, *J. Atmos. Chem.*, **41**, 109–134, 2002.
- Díaz, J. P., F. J. Expósito, C. J. Torres, F. Herrera, J. M. Prospero, and M. C. Romero, Radiative properties of aerosols in Saharan dust outbreaks using ground-based and satellite data: Applications to radiative forcing, *J. Geophys. Res.*, **106**, 18,403–18,416, 2001.
- Dickerson, R. R., S. Kondragunta, G. Stenchikov, K. L. Civerolo, B. G. Doddridge, and B. N. Holben, The impact of aerosols on solar ultraviolet radiation and photochemical smog, *Science*, **278**, 827–830, 1997.
- Diner, D. J., et al., MISR aerosol optical depth retrievals over southern Africa during the SAFARI-2000 dry season campaign, *Geophys. Res. Lett.*, **28**, 2130–2137, 2001.
- Dubovik, O., B. Holben, T. F. Eck, A. Smirnov, Y. J. Kaufman, M. D. King, D. Tanré, and I. Slutsker, Variability of absorption and optical properties of key aerosol types observed in worldwide locations, *J. Atmos. Sci.*, **59**, 590–608, 2002.
- Giorgi, F., and W. L. Chameides, Rainout lifetimes of highly soluble aerosols and gases as inferred from simulations with a general circulation model, *J. Geophys. Res.*, **91**, 14,367–14,376, 1986.
- Grams, G. W., I. H. Blifford, D. A. Gillette Jr., and P. B. Russell, Complex index of refraction of airborne soil particles, *J. Appl. Meteorol.*, **13**, 459–471, 1974.
- Hall, T. M., and M. J. Prather, Simulations of the trend and annual cycle in stratospheric CO₂, *J. Geophys. Res.*, **98**, 10,573–10,581, 1993.
- Hannegan, B., S. Olsen, M. Prather, X. Zhu, D. Rind, and J. Lerner, The dry troposphere: A limit on cometary water influx, *Geophys. Res. Lett.*, **25**, 1649–1652, 1998.
- He, S., and G. R. Carmichael, Sensitivity of photolysis rates and ozone production in the troposphere to aerosol properties, *J. Geophys. Res.*, **104**, 26,307–26,324, 1999.
- Higurashi, A., T. Nakajima, B. Holben, A. Smirnov, R. Frouin, and B. Chatenet, A study of global aerosol optical climatology with two-channel AVHRR remote sensing, *J. Clim.*, **13**, 2011–2027, 2000.
- Hook, S. J., J. J. Myers, K. J. Thome, M. Fitzgerald, and A. B. Kahle, The MODIS/ASTER airborne simulator (MASTER)—A new instrument for earth science studies, *Remote Sens. Environ.*, **76**, 93–102, 2001.
- Hsu, N. C., J. R. Herman, O. Torres, B. N. Holben, D. Tanre, T. F. Eck, A. Smirnov, B. Chatenet, and F. Lavenu, Comparisons of the TOMS aerosol index with Sun-photometer aerosol optical thickness: Results and applications, *J. Geophys. Res.*, **104**, 6269–6279, 1999.
- Jacob, D. J., Heterogeneous chemistry and tropospheric ozone, *Atmos. Environ.*, **34**, 2131–2159, 2000.
- Jacob, D. J., S.-M. Fan, S. C. Wofsy, P. A. Spiro, P. S. Bakwin, J. A. Ritter, E. V. Browell, G. L. Gregory, D. R. Fitzjarrald, and K. E. Moore, Deposition of ozone to tundra, *J. Geophys. Res.*, **97**, 16,473–16,479, 1992.
- Jacob, D. J., et al., Evaluation and intercomparison of global atmospheric transport models using ²²²Rn and other short-lived tracers, *J. Geophys. Res.*, **102**, 5953–5970, 1997.
- Jacobson, M. Z., Studying the effects of aerosols on vertical photolysis rate coefficient and temperature profiles over an urban airshed, *J. Geophys. Res.*, **103**, 10,593–10,604, 1998.
- Ji, Q., S. Tsay, R. Hansell, and P. Pilewskie, SMART ground-based radiation measurements during PRIDE, *Eos Trans. AGU*, **81**(48), Fall Meet. Suppl., Abstract A51E-07, 2000.
- Kaufman, Y. J., D. Tanré, O. Dubovik, A. Karnieli, and L. A. Remer, Absorption of sunlight by dust as inferred from satellite and ground-based remote sensing, *Geophys. Res. Lett.*, **28**, 1479–1482, 2001.
- Kinne, S., et al., Monthly averages of aerosol properties: A global comparison among models, satellite data, and AERONET ground data, *J. Geophys. Res.*, **108**, doi:10.1029/2001JD001253, in press, 2003.
- Knapp, K. R., and L. L. Stowe, Evaluating the potential for retrieving aerosol optical depth over land from AVHRR Pathfinder atmosphere data, *J. Atmos. Sci.*, **59**, 279–293, 2002.
- Knipping, E. M., M. J. Lakin, K. J. Foster, P. Jungwirth, D. J. Tobias, R. B. Gerber, D. Dabdub, and B. J. Finlayson-Pitts, Experiments and simulations of ion-enhanced interfacial chemistry on aqueous NaCl aerosols, *Science*, **288**, 301–306, 2000.
- Lary, D. J., M. P. Chipperfield, R. Toumi, and T. Lenton, Heterogeneous atmospheric bromine chemistry, *J. Geophys. Res.*, **101**, 1489–1504, 1996.
- Lary, D. J., D. E. Shallcross, and R. Toumi, Carbonaceous aerosols and their potential role in atmospheric chemistry, *J. Geophys. Res.*, **104**, 15,929–15,940, 1999.
- McLinden, C. A., S. C. Olsen, B. Hannegan, O. Wild, M. J. Prather, and J. Sundet, Stratospheric ozone in 3-D models: A simple chemistry and the cross-tropopause flux, *J. Geophys. Res.*, **105**, 14,653–14,665, 2000.
- Mishchenko, M. M., I. Geogdzhayev, B. Cairns, W. Rossow, and A. Lacis, Aerosol retrievals over the ocean by use of channels 1 and 2 AVHRR data: Sensitivity analysis and preliminary results, *Appl. Opt.*, **38**, 7325–7341, 1999a.
- Mishchenko, M. M., J. Dlugach, E. Yanovitskij, and N. Zakharova, Bidirectional reflectance of flat, optically thick particulate layers: An efficient radiative transfer solution and applications to snow and soil surfaces, *J. Quant. Spectrosc. Radiat. Transfer*, **63**, 409–432, 1999b.
- Mishchenko, M. M., L. D. Travis, and A. A. Lacis, *Scattering, Absorption, and Emission of Light by Small Particles*, Cambridge Univ. Press, New York, 2002.
- Olsen, S. C., B. J. Hannegan, X. Zhu, and M. J. Prather, Evaluating ozone depletion from very short-lived halocarbons, *Geophys. Res. Lett.*, **27**, 1475–1478, 2000.
- Olson, J., et al., Results from the Intergovernmental Panel on Climatic Change Photochemical Model Intercomparison (PhotoComp), *J. Geophys. Res.*, **102**, 5979–5991, 1997.
- Penner, J. E., et al., A comparison of model- and satellite-derived aerosol optical depth and reflectivity, *J. Atmos. Sci.*, **59**, 441–460, 2002.
- Prather, M. J., and D. Ehhalt, Atmospheric chemistry and greenhouse gases, in *Climate Change 2001, the Scientific Basis*, edited by J. E. A. Houghton, pp. 239–288, Cambridge Univ. Press, New York, 2001.
- Prather, M. J., M. McElroy, S. Wofsy, G. Russell, and D. Rind, Chemistry of the global troposphere: Fluorocarbons as tracers of air motion, *J. Geophys. Res.*, **92**, 6579–6613, 1987.
- Savoie, D. L., H. Maring, M. Izaguirre, T. Snowdon, and L. Custals, Ground-based measurements of aerosol chemical, physical, and optical properties during the Puerto Rico Dust Experiment (PRIDE), *Eos Trans. AGU*, **81**(48), Fall Meet. Suppl., Abstract A51E-10, 2000.
- Stowe, L. L., A. M. Ignatov, and R. R. Singh, Development, validation, and potential enhancements to the second-generation operational aerosol product at the National Environmental Satellite, Data, and Information Service of the National Oceanic and Atmospheric Administration, *J. Geophys. Res.*, **102**, 16,923–16,934, 1997.
- Takemura, T., H. Okamoto, Y. Maruyama, A. Numaguti, A. Higurashi, and T. Nakajima, Global three-dimensional simulation of aerosol optical thickness distribution of various origins, *J. Geophys. Res.*, **105**, 17,853–17,873, 2000.

- Takemura, T., T. Nakajima, O. Dubovik, B. N. Holben, and S. Kinne, Single-scattering albedo and radiative forcing of various aerosol species with a global three-dimensional model, *J. Clim.*, *15*, 333–352, 2002.
- Tie, X., G. Brasseur, L. Emmons, L. Horowitz, and D. Kinnison, Effects of aerosols on tropospheric oxidants: A global model study, *J. Geophys. Res.*, *106*, 22,931–22,964, 2001.
- Torres, O., P. K. Bhartia, J. R. Herman, A. Sinyuk, P. Ginoux, and B. Holben, A long-term record of aerosol optical depth from TOMS observations and comparison to AERONET measurements, *J. Atmos. Sci.*, *59*, 398–413, 2002.
- Twitty, J. T., and J. Weinman, Radiative properties of carbonaceous aerosols, *J. Appl. Meteorol.*, *10*, 725–731, 1971.
- Underwood, G. M., C. H. Song, M. Phadnis, G. R. Carmichael, and V. H. Grassian, Heterogeneous reactions of NO₂ and HNO₃ on oxides and mineral dust: A combined laboratory and modeling study, *J. Geophys. Res.*, *106*, 18,055–18,066, 2001.
- Volz, F. E., Infrared refractive index of atmospheric aerosol substances, *Appl. Opt.*, *11*, 755–759, 1972.
- Wahner, A., T. F. Mentel, M. Sohn, and J. Stier, Heterogeneous reaction of N₂O₅ on sodium nitrate aerosol, *J. Geophys. Res.*, *103*, 31,103–31,112, 1998.
- Ward, G., K. Cushing, R. McPeters, and A. Green, Atmospheric aerosol index of refraction and size-altitude distribution from bistatic laser scattering and solar aureole measurements, *Appl. Opt.*, *12*, 2585–2592, 1973.
- Wild, O., and H. Akimoto, Intercontinental transport of ozone and its precursors in a three-dimensional global CTM, *J. Geophys. Res.*, *106*, 27,729–27,744, 2001.
- Wild, O., and M. J. Prather, Excitation of the primary tropospheric chemical mode in a global three-dimensional model, *J. Geophys. Res.*, *105*, 24,647–24,660, 2000.
- Wild, O., X. Zhu, and M. Prather, Fast-J: Accurate simulation of in- and below-cloud photolysis in tropospheric chemical models, *J. Atmos. Chem.*, *37*, 245–282, 2000.

H. Bian and M. J. Prather, Department of Earth System Science, University of California, 1 Physical Sciences Road, Irvine, CA 92697-3100, USA. (hbian@uci.edu; mprather@uci.edu)

T. Takemura, Research Institute for Applied Mechanics, Kyushu University, Fukuoka, Japan, 6-1 Kasuga-koen, Kasuga, Fukuoka 816-8580, Japan. (toshi@riam.kyushuu.ac.jp)

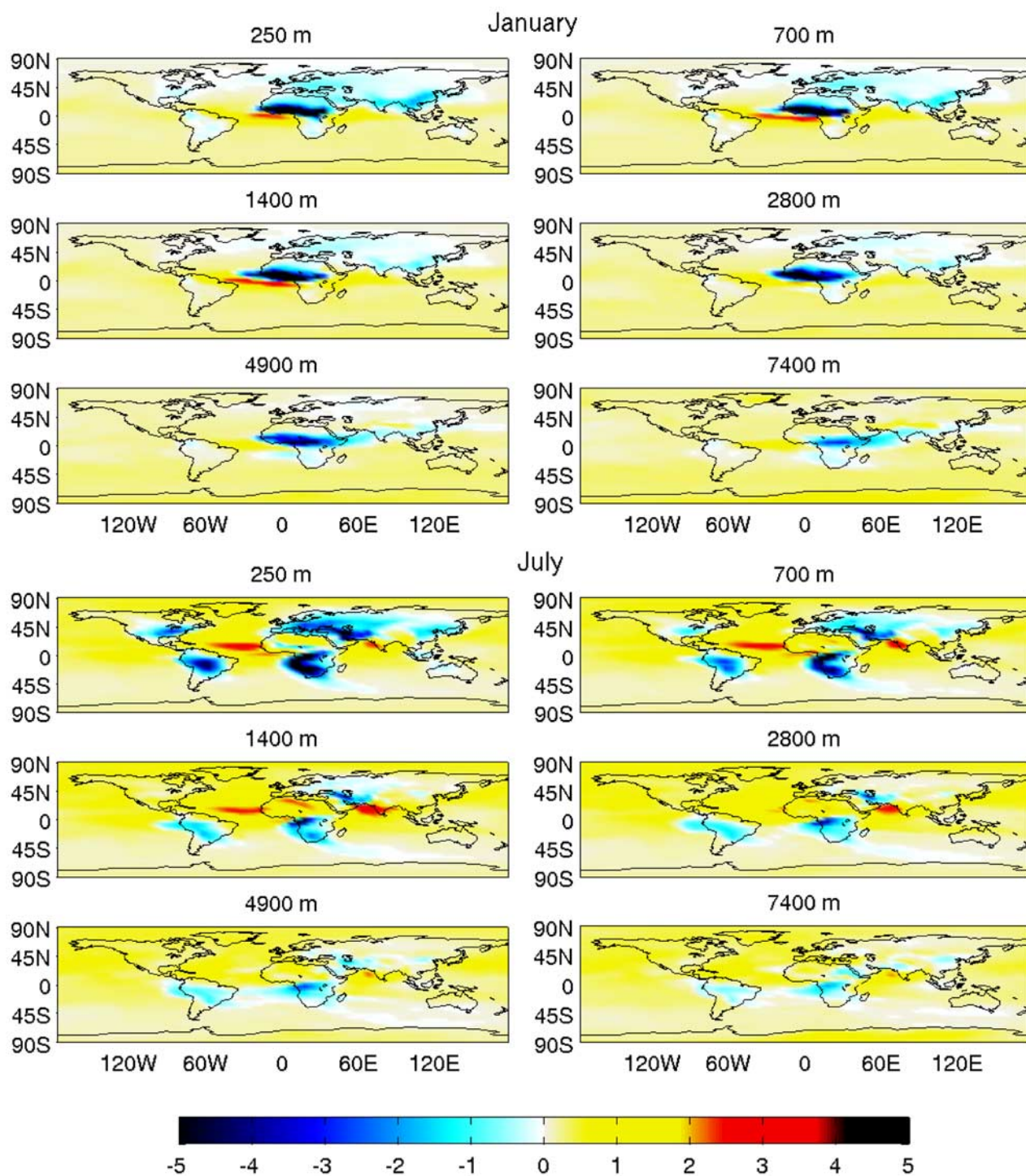


Figure 3. Perturbations to O₃ (ppb) by global aerosol at six atmospheric layers in January and July.